Error Compensation by Sensor Re-calibration in Fringe Projection Based Optical 3D Stereo Scanners

Christian Bräuer-Burchardt, Peter Kühmstedt, and Gunther Notni

Fraunhofer Institute Applied Optics and Precision Engineering, Jena, Germany
{christian.braeuer-burchardt,peter.kuehmstedt,
gunther.notni}@iof.fraunhofer.de

Abstract. A new methodology for the determination and correction of calibration errors in optical 3D scanners is introduced. The accuracy of optical 3D scanners is reduced when calibration parameters are no longer valid caused by e.g. changes of temperature or mechanic influences. Whereas complete new calibration of a system may be impossible or too expensive, a compensation of the parameter errors can lead to acceptable results. The new method is based on measurement of a simple grid pattern or arbitrary measuring objects. Results show that the method provides acceptable results concerning point correspondence and scaling error compensation. It takes low effort and is easy to handle.

Keywords: camera calibration, epipolar geometry, fringe projection.

1 Introduction

High precision measuring systems based on image data require high precision optical components. Measuring accuracy, however, depends additionally on the quality of the geometric description of the components. Geometry determination of a 3D scanning system is performed in the process of camera calibration. Its correctness is crucial for the quality of a photogrammetric system and essential for its measuring accuracy.

Contactless 3D-measuring systems are increasingly used for industrial, medical, archaeological, and other applications. The requirements according measurement accuracy are growing while the handling should become easier. Modern photogrammetric measurement systems based on active structured light projection achieve measurement accuracies of up to 1:100000 compared to the length extension of the measuring field [1]. However, such high accuracies can only be achieved, if geometry of the measuring system is stable over time between calibration and measurement. This is, unfortunately, only the case, if certain measurement conditions strictly hold. However, in practical use this cannot always be ensured (see e.g. [2] or [3]).

Previous work has been dealt with the stability of camera calibration, e.g. by Läbe and Förstner [4], Habib et al. [5], and Rieke-Zapp et al. [3]. Zhang [6] gives an extensive review of the uncertainty of the epipolar geometry. A detailed description of the sensitivity of the 3D reconstruction depending on erroneous calibration parameters is presented by Dang et al. [7].

G. Maino and G.L. Foresti (Eds.): ICIAP 2011, Part II, LNCS 6979, pp. 363–373, 2011.

Our goal was to develop a method which compensates measurement errors of optical 3D sensors caused by thermic instability or mechanic influences by correction of calibration parameters. Two novel methodologies for calibration analysis and correction are introduced. The first corrects those parameters leading to point correspondence errors. The second one additionally compensates scaling and deformation errors.

2 Measuring Principles

2.1 Phasogrammetry

Phasogrammetry is the mathematical connection of photogrammetry and fringe projection. The classical approach of fringe projection is described e.g. by Schreiber and Notni [8], which has been extended depending on several applications (see [9, 10]). The principle should be briefly explained as follows. A fringe projection unit projects one or two perpendicular, well defined fringe sequences onto the object, which is observed by one ore more cameras. These sequences may consist of a binary code sequence as the Gray code (see [11, 12]) and a sequence of up to 16 sinusoidal fringe patterns. The so called rough phase value [8], and in combination with the Gray code the unique phase value [11] is obtained using a sequence of sinusoidal pattern. Unique phase values are used to realize point correspondences in order to obtain measurement values by triangulation (see [1]).

2.2 Stereo Vision and Epipolar Geometry

Using active stereo vision, images of the object are captured from two different perspectives. Pairs of image coordinates resulting from the same object point (the homologous points) have to be identified. The object can be reconstructed by triangulation [1] using these points. In the case of active stereo vision a single intensity pattern or a sequence of patterns is projected onto the object under measure. There are several techniques to identify the homologous points in both cameras (see e.g. [1]).

Epipolar geometry is a well-known principle which is often used in photogrammetry when stereo systems are present. See for example [1]. It is characterized by an arrangement of two cameras observing almost the same object scene. A measuring object point M defines together with the projection centres O_1 and O_2 of the cameras a plane E in the 3D space. The images of E are corresponding epipolar lines concerning M. When the image point m of M is selected in the image I_1 of camera C_1, the corresponding point m_2 in the image I_2 of camera C_2 must lie on the corresponding epipolar line. This restricts the search area in the task of finding corresponding points.

In the following we assume a system consisting of two cameras C_1 and C_2 and one projector in a fixed arrangement.

2.3 Camera Calibration

Camera calibration means the determination of the intrinsic and extrinsic parameters (including lens distortion parameters) of an optical system. It has been extensively described in the literature, e.g. in [1, 10, 13]. Different principles are performed to

conduct camera calibration. The selection depends on the kind of the optical system, the exterior conditions, the effort to be pushed, and the desired measurement quality. In case of the calibration of photogrammetric stereo camera pairs, the intrinsic parameters (principal length, principal point, and distortion description) of both cameras should be determined as well as the relative orientation between the cameras.

The position of the camera in the 3D coordinate system is described by the position of the projection centre O = (X, Y, Z) and a rotation matrix R obtained from the three orientation angles ω, ϕ, and κ. Considering stereo camera systems, the relative orientation between the two cameras (see [1]) should be considered, because the absolute position of the stereo sensor is usually out of interest.

Lens distortion may be considerable and should be corrected by a distortion correction operator D. Distortion may be described by distortion functions or by a field of selected distortion vectors (distortion matrix). The determination of D may be performed within the calibration procedure or separately (see e.g. [14]).

3 Fringe Projection Based 3D Stereo Scanners

3.1 Situation

Let a fringe projection based 3D stereo scanner following the principles described in the previous section be given. It takes one sequence of images from each measuring position. This requires a preliminary calibration of the sensor. Two application modes are distinguished.

First, two sequences of Gray code and sinusoidal images rotated by 90°, respectively, are projected and observed leading to two phase images (see [5]). An algorithm using phase correlation is used to identify the corresponding points in the image of camera C_2 to the given points with integer coordinates in the image of camera C_1. This mode should be denoted by m_1 mode.

Second mode, denoted by m_1 uses the epipolar geometry. The corresponding point q in the image of camera C_2 for a given point $p = (x, y)$ in the image of camera C_1 is found by search on the epipolar line defined by p and the relative orientation between the stereo camera pair. This requires the projection of only one sequence of Gray code and sinusoidal images. This mode should be denoted by m_2 mode. In the following we use mode m_2 for image acquisition as it is much faster compared to m_1.

Assume that all calibration parameters including distortion description D_1 and D_2 have been obtained by a suitable calibration process. The other parameters are X_1, Y_1, Z_1, ω_1, ϕ_1, κ_1, c_1, u_1, v_1, X_2, Y_2, Z_2, ω_2, ϕ_2, κ_2, c_2, u_2, and v_2, where (X_i, Y_i, Z_i) are the projection centres, ω_i, ϕ_i, and κ_i are the orientation angles, resulting in the rotation matrices R_i, c_i are the principal distances, and (u_i, v_i) are the principal points of the two cameras (i = 1, 2).

3.2 Stability of the Measurement

The measuring accuracy of a calculated 3D point using triangulation depends on several aspects. In the ideal case, calibration data is error free and positions of the found corresponding points are located perfectly. Then triangulation provides a proper

intersection of the two rays r_1 and r_2 and the position error of the reconstructed point *M'* is zero. However, the calculated position *M'* will be erroneous due to the position error of q in the image of camera C_2 and the calibration data error. The position error of q depends on phase noise and a location error of the epipolar line. Whereas phase noise is a random error with typically normal distribution which can be statistically estimated, location error depends on the quality of calibration including distortion correction and the triangulation angle.

Because calibration is performed preliminary and is not updated during measurement cycles, the calibration parameters have to be stable in order to achieve constant good measurement accuracy. However, changes of temperature and mechanic influences as e.g. vibrations or shocks may considerably disturb the geometry of the sensor [3]. In that case current calibration data becomes erroneous leading to errors in the 3D data outcome. Unfortunately, the amount of these errors is difficult to estimate, e.g. in the case of mechanic shocks as the deviation of the calibration parameter is usually unknown. Performing a complete calibration update of the sensor is usually impracticable as it is time consuming, needs a sophisticated operator, and can often not be performed in the working position of the sensor. However, if the error of the current measurement is considerable, but unknown, the measurement result becomes useless.

In the case of fringe projection based 3D sensors operating temperatures often are significantly higher than the temperature of the environment, which might lead to a significant error. This error mainly results in a position error of corresponding points used for triangulation, and a scaling or deformation error due to invalid calibration parameter set. In the following section we introduce an approach to compensate for such errors using a low effort single shot measurement method.

Hand held, mobile, and moved sensors are additionally exposed to mechanic influences as shocks or vibrations which may disturb the calibration data.

4 Approach of Error Compensation

As mentioned above, there are two major problems concerning a disturbed sensor calibration. First, disturbed calibration leading to erroneous measurement results has to be detected. Second, considerable disturbances have to be corrected for. Hence our approach consists of two parts: detection and correction. The method should be applicable in the measurement modus of the sensor. It has not to require considerable effort, but easy to handle and being automated. It should realize a correction of calibration data such, that measurement errors are sufficiently reduced.

The approach was performed following two strategies. First, compensation procedure should be extremely simple and robust while the effort must be minimal. This leads to the concept of epipolar line correction (ELC). Second, calibration error has to be compensated by most accurate correction of the calibration parameters.

4.1 Simulation and Correction Model

To simplify the development of an automated method which compensates for errors due to thermal drift of the calibration parameters with low effort, not all of the 18 calibration parameters are considered. Instead, the most contributing parameters are

selected. Analysis of the parameter error influence has been performed for identification. Let us consider first the epipolar line position error $err_{pos}(p,q)_i$, which should be defined as the perpendicular distance of the correct corresponding point q_i to the epipolar line defined by the set of calibration parameters. The mean epipolar line error ΔE_{mn} and the rms epipolar line error ΔE_{rms} of the image pair are defined by

$$\Delta E_{mn} = \frac{1}{n}\sum_{i=1}^{n} err_{pos}(p,q)_i \quad \text{and} \quad \Delta E_{rms} = \sqrt{\frac{1}{n}\sum_{i=1}^{n}\left(err_{pos}(p,q)_i\right)^2}\,, \tag{1}$$

respectively, where n is the number of corresponding point pairs which should be well distributed over the images. Additionally, the maximal epipolar line error ΔE_{max} may be considered: $\Delta E_{max} = \max\{\,|\,err_{pos}(p,q)_i\,|\}$.

The epipolar line error according to (1) is similar to the measure defined by Zhang to compare fundamental matrices obtained by different calibration procedures [6].

The influence of the different calibration parameters to ΔE_{rms} was determined as follows. A set of parameters similar to those of a real sensor [15] was constructed and a plane measuring object was simulated. This simulation provides well defined results of reconstructed 3D points. Then, a manipulation of every single calibration parameter was performed in order to estimate its influence on the mean epipolar line error ΔE_{rms}.

The set of parameters can be reduced due to symmetric effects of the parameters (e.g. an error of ΔX_1=0.1mm should have the same effect as $\Delta X_2 = -0.1$ mm) leading to $X_2, Y_2, Z_2, \omega_2, \varphi_2, \kappa_2, c_2, u_2, v_2$ as the considered parameters. In the following the index '$_2$' will be omitted. The nine parameters were disturbed with a reasonable error.

Table 1 shows the result of the mean epipolar line error and fig. 1 illustrates the distribution of selected error vectors. It can be seen that some of the parameters have a low effect on ΔE, e.g. X, ϕ, and κ: For some other parameters, the effects are very similar to each other (Y, ω, and v) concerning ΔE. Hence some of the parameters may be omitted when only the epipolar line error is considered in order to simplify the algorithm of finding the correction values. The effect of the parameter errors on the 3D data can be calculated by triangulation. It is also described by Dang et al. [7].

Unfortunately, epipolar line error ΔE is only sensitive in direction perpendicular to the epipolar lines. If the current calibration is disturbed by e.g. ΔX or $\Delta\phi$, this will hardly be detected by only analysing ΔE. Hence scaling error $\Delta S(P,Q)$ is defined by

$$\Delta S(P,Q) = \frac{\overline{PQ_{meas}} - \overline{PQ_{corr}}}{\overline{PQ_{corr}}} \tag{2}$$

where $\overline{PQ_{corr}}$ is the correct distance between two 3D points P and Q and $\overline{PQ_{meas}}$ is the measured distance between P and Q.

Analysis of the influence on scaling error was performed analogously to the analysis of the epipolar line error. The scaling error as function of the position of the points in the image was provided by simulation. Four regions (for the selected points P and Q) for the analysis were defined: horizontal above A, horizontal below B, vertical left C, and vertical right D, corresponding to long distant length measurements close to

the margins of the measurement field. Mean absolute scaling error ΔS_{mna} with sum of non-negative weights equal to one ($w_A + w_B + w_C + w_D = 1$) is defined by

$$\Delta S_{mna} = \frac{w_A}{n_A}\sum_{i=1}^{n_A}\left|\Delta S_{Ai}\right| + \frac{w_B}{n_B}\sum_{i=1}^{n_B}\left|\Delta S_B i\right| + \frac{w_C}{n_C}\sum_{i=1}^{n_C}\left|\Delta S_{Ci}\right| + \frac{w_D}{n_D}\sum_{i=1}^{n_D}\left|\Delta S_{Di}\right| \cdot \tag{3}$$

Table 1. Epipolar line error ΔE depending on calibration parameter errors (examples)

parameter	X	Y	Z	ϕ	ω	κ	c	u	v
Δparameter	0.1mm	0.1mm	0.1mm	0.05°	0.05°	0.05°	0.1mm	0.01 mm	0.01mm
ΔE_{rms} [pixel]	0,03	2.62	0.28	0.08	3.88	0.11	0.65	0.02	2.08
ΔE_{max} [pixel]	0,07	2.66	0.42	0.14	3.93	0.20	1.28	0.05	2.12

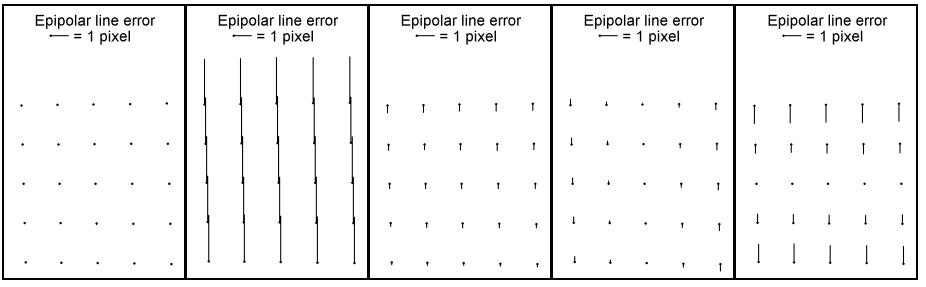

Fig. 1. Epipolar line error ΔE in dependence on selected single calibration parameter errors: ΔX_2= 0.1 mm, ΔY_2= 0.1 mm, ΔZ_2= 0.1 mm, $\Delta\kappa_2 = 0.1°$, and $\Delta c_2 = -0.1$ mm (from left to right)

4.2 Correction Approaches

For error compensation in a disturbed measurement we suggest two strategies. The first one should be denoted by epipolar line error correction (ELC) and can be obtained either by correction of the epipolar line positions or by calibration parameter manipulation. It shifts the epipolar lines according to the measured epipolar line error ΔE_{rms}. This leads to correct 2D coordinates of corresponding points resulting in prevention of locally appearing 3D errors. The advantage of this approach is a simple and fast determination, even applicable in the measurement process of arbitrary measuring objects. (The proposed grid pattern is not necessary!). However, scaling errors and deformations due to erroneous calibration cannot be corrected.

The second approach, denoted by calibration parameter correction (CPC), realizes a correction of all selected calibration parameters according to the minimization of ΔE_{rms} and ΔS_{mna} and includes the correction of point correspondences as well as the correction of scaling errors and deformations.

4.3 Selection of the Parameters

A set of relevant calibration parameters is selected according to the selected approach (ELC or CPC). This can be done after analysis of the errors ΔE and ΔS by performing

a reference measurement. Alternatively, a heuristically found default parameter set (e.g. Y_2, Z_2, κ_2 or ω_2, Z_2, κ_2 for ELC and X_2, Y_2, Z_2, ϕ_2, ω_2 , κ_2 , c_2 for CPC) can be chosen.

The coordinates of the principal points u_1, v_1, u_2, and v_2 were omitted for both epipolar line error and scaling error estimation as the errors of u_1, v_1, u_2, and v_2 are assumed to be small in relation to those of the extrinsic parameters. Additionally, the remaining errors may be partly compensated by the selected correction parameters due to correlation effects.

4.4 Pure Determination of the Epipolar Line Error

In order to determine exclusively the epipolar line error, a measurement of an arbitrary measuring object is performed by the sensor using the m_1 mode. A number of points (e.g. 80 to 200) arranged in a rectangular grid covering the whole image field must be selected in the image of camera C_1 as reference point set. Selection criterion should be minimal position error probability. Erroneous point correspondences $(p, q)_i$ are determined on the epipolar lines. Second phase direction is used to estimate the correct point correspondences $(p', q')_i$. The epipolar line error is estimated by the difference of q_i and q'_i in direction perpendicular to the epipolar lines.

4.5 Determination of the Scaling Error

Scaling error determination is proposed as follows. A rectangular plane grid may be used with known exact distances between the grid points. The coordinates of the grid points are determined with high sub-pixel accuracy. Length measurements l_i are performed using selected points. Measurement results are compared to the correct distances l_i^{ref} leading to four values ΔS_A, ΔS_B, ΔS_C, and ΔS_D of ΔS according to (3).

4.6 Determination of the Correction Parameters

The set of point correspondences $(p, q)_i$ obtained by the reference measurement, and four point correspondences for length measurement are the input for the algorithm of the correction parameter estimation. A test quantity $\Delta T = f_E \cdot \Delta E_{rms} + f_S \cdot \Delta S_{mna}$ with $f_E + f_S = 1$ to be minimized is defined, where f_E and f_S are meaningful, heuristically set scaling factors which can be obtained by experiments. The accuracy of the scaling error determination depends on the precision of the used grid and the grid point localization accuracy. If scaling error ΔS_{mna} should be neglected, $f_S = 0$ may be set leading to reduced parameter set and faster re-calibration.

The selected m parameters are changed systematically by addition of $k \cdot \delta par_j$, j=1,…,m, where $k = -1, 0, +1$, and $\delta par_j = (\delta X, \delta Y , \delta Z, \delta\phi, \delta\omega, \delta\kappa;$ *and* $\delta c)$, respectively. The initial value for the δpar_j are set to meaningful, heuristically obtained values, e.g. 0.1 mm for X, Y, and Z, and 0.01° for ω, ϕ, and κ. The test quantity ΔT is determined for all 3^m combinations of $k \cdot \delta par_j$. The minimum $\Delta T_{min} = \min \{\Delta T_j (p,q)_i\}$, j=1,…, 3^m defines the favourite combination of the manipulated parameters. Depending on whether it holds $k_j \neq 0$ or $k_j = 0$ the δpar_j do not change or are devided by two, respectively: $\delta par_j := \delta par_j / 2$. The calculation of ΔT is iterated until no improvement of ΔT occurs or the maximum number of iterations is achieved.

4.7 Selection of the Correction Strategy

According to the factors f_E and f_S the influence of the epipolar line error or the scaling error, respectively, dominates. Actually, the use of only the scaling error (i.e. $f_E = 0$) would be sufficient in order to correct the calibration parameters. However, $f_E = 0$ leads to worse results than in the case $f_E > 0$ which has been verified by experiments (see next section). Additionally, using fringe projection systems the epipolar line error can be usually determined with low uncertainty. The accuracy of ΔS determination depends on the precision of the grid pattern measurement and may be lower than determination of ΔE. Hence epipolar line error should be always considered.

5 Results

5.1 Analysis of Thermic Behaviour

First we analysed a 3D stereo sensor (called DS) based on fringe projection which is used for intraoral measurements [15]. It observes a measurement field of about 20 mm x 15 mm. The depth of the measuring volume is about 12 mm. Image size is 516 x 778 pixel. Due to the absence of active ventilation and cooling the electronic components lead to a significant increase of the operating temperature to more than 30°C. Hence an influence of the changing temperature on the measuring accuracy is expected.

The following measurements were performed. First, only the epipolar line error was investigated. Therefore a white plane surface was measured using mode m_1 (see section 3.1). Epipolar line error ΔE_{rms} was determined and the estimation of the correction parameters Y_2, Z_2, and κ_2 was performed as described in section 4. The resulting parameter values were used to correct the location of the epipolar lines. The results before and after correction for one selected but representative measurement are documented in fig. 2 (left).

The same procedure was performed using the reference grid object. Parameters X_2, ω_2, ϕ_2, and c_2 were additionally included into the compensation. Results are given in table 2 and illustrated in fig. 2 (right). Note that the temperature caused (uncorrected) errors ΔE and ΔS are minimal at about 30 min after switching on the system. Thereafter, uncorrected errors increase again. After correction, however, epipolar line error is always below 0.06 pixel, and scaling error is below 0.15 %.

Table 2. Thermic drift influenced ΔE and ΔS measurement. $\Delta E'$ and $\Delta S'$ are corrected values

time \ error	ΔE_{rms} [pixel]	$\Delta E'_{rms}$ [pixel]	ΔE_{max} [pixel]	$\Delta E'_{\max}$ [pixel]	ΔS_{mna} [%]	$\Delta S'_{mna}$ [%]
0 min	0,68	0,06	0,85	0,31	1,38	0,14
10 min	0,08	0,03	0,23	0,17	0,90	0,12
20 min	0,10	0,02	0,15	0,10	0,25	0,09
30 min	0,05	0,05	0,17	0,15	0,07	0,06
60 min	0,36	0,03	0,50	0,15	0,08	0,06
90 min	0,44	0,03	0,53	0,09	0,11	0,10

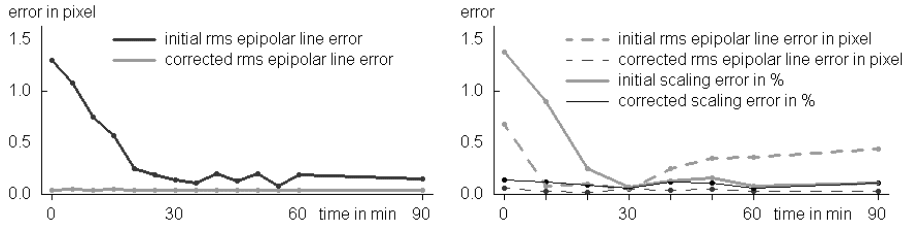

Fig. 2. Temperature influenced error ΔE (left) and both ΔE and ΔS (right) of DS over 90 min

5.2 Detection of Mechanic Influences

Next, the long-term behaviour of the stability of the calibration data of different flexible sensors was analysed. Evaluation of ΔE_{rms} was performed at different days over a period of several weeks. Exceptions after certain (but unknown) events are possible which require a sensor re-calibration as proposed. See an example in fig. 3 showing a relative high stability over three weeks. Then, a (probably) mechanic shock disturbed the calibration of the sensor at day 21. The effect of this change to a measurement of a prism in the unhandled 3D measurement and corrected result is also shown in fig. 3.

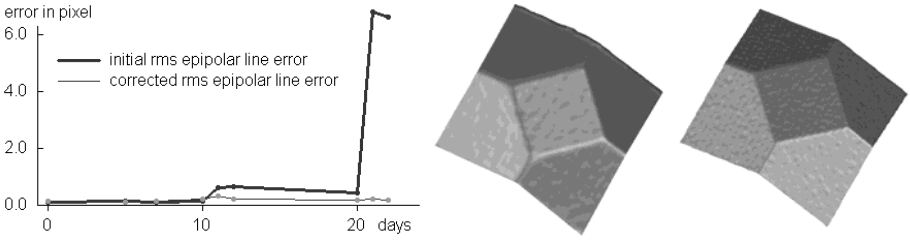

Fig. 3. Result of long-term behavior of ΔE (left) and influence of the sudden error on the 3D measurement of a prism: erroneous result with blurred edges (middle) and result after re-calibration (right)

5.3 Weight Optimization

As already mentioned in section 4.7, consideration of ΔS leads to ΔE being redundant. However, experiments with omission of ΔE did not show the desired results. Hence, experiments with varying ratio between f_E and f_S were performed using a representative dataset of our scanner DS. A three-parameter (Y_2, Z_2, κ_2) and a seven-parameter (X_2, Y_2, Z_2, ϕ_2, ω_2, κ_2, c_2) manipulation of the calibration parameters were performed.

The results are documented in table 3. Initial epipolar line error was $\Delta E_{rms} = 0.68$ and scaling error 1.39 according to (1) and (2). Whereas three-parameter manipulation gives almost constant ΔS error and a low ΔE value after correction for values $f_E > 0.1$ and considerable ΔE error for $f_E \leq 0.1$. Seven-parameter manipulation gives acceptable results in the range of $0.1 \leq f_E \leq 0.9$. Hence, if ΔS determination is omitted,

three-parameter manipulation should be performed and ΔE must not be omitted at all. If scaling error can be determined sufficiently accurate, seven-parameter manipulation should be performed with about $f_E = 0.3$ and $f_S = 0.7$.

Table. 3. Epipolar line and scaling error after three-parameter (Y_2, Z_2, κ_2) manipulation (left) and seven-parameter (X_2, Y_2, Z_2, ϕ_2, ω_2, κ_2, c_2) manipulation (right) depending on f_E and f_S

f_E	f_S	ΔE^3_{rms} [pixel]	ΔS^3_{mna} [%]	ΔE^7_{rms} [pixel]	ΔS^7_{mna} [%]
0.00	1.00	51,85	0,99	14,00	0,10
0.01	0.99	0,99	1,05	0,13	0,10
0.10	0.90	0,88	1,06	0,11	0,10
0.30	0.70	0,07	1,37	0,10	0,11
0.50	0.50	0,10	1,43	0,06	0,14
0.70	0.30	0,10	1,43	0,04	0,16
0.90	0.10	0,05	1,38	0,04	0,17
0.99	0.01	0,06	1,39	0,04	0,18
1.00	0.00	0,06	1,39	0,04	4,00

6 Summary, Discussion, and Outlook

A new methodology for sensor re-calibration and compensation calibration errors of stereo 3D scanners based on fringe projection technique was introduced. These errors are due to the thermic state of the sensor or mechanic influences. The method requires minimal effort and allows a sufficient correction of the distorted measuring results. The technique needs only a one position measurement of an arbitrary object or a grid pattern with known lengths between certain points, respectively.

The results show, that thermic drift or mechanic shocks may lead to considerable errors in the point correspondence finding which may be corrected adequately.

Due to high correlation between the calibration parameters, re-calibration based on the proposed method does not necessarily find the set of “true” parameters. Hence, further analysis of the parameter influence and searching for a better separation of these influences will be addressed in further work. Additionally, the proposed method should be tested on more different scanner systems.

References

1. Luhmann, T., Robson, S., Kyle, S., Harley, I.: Close range photogrammetry. Wiley Whittles Publishing, Chichester (2006)
2. Hastedt, H., Luhmann, T., Tecklenburg, W.: Image-variant interior orientation and sensor modelling of high-quality digital cameras. IAPRS 34(5), 27–32 (2002)
3. Rieke-Zapp, D., Tecklenburg, W., Peipe, J., Hastedt, H., Haig, C.: Evaluation of the geometric stability and the accuracy potential of digital cameras – Comparing mechanical stabilisation versus parameterisation. ISPRS Journal 64/3, 248–258 (2009)
4. Läbe, T., Förstner, W.: Geometric Stability of Low-Cost Digital Consumer Cameras. In: Proc. ISPRS, pp. 528–535 (2004)
5. Habib, A.F., Pullivelli, A.M., Morgan, M.F.: Quantitative measures for the evaluation of camera stability. Opt. Eng. 44, 033605-1– 033605-8 (2005)

6. Zhang, Z.: Determining the epipolar geometry and its uncertainty: a review. IJCV 27(2), 161–198 (1998)
7. Dang, T., Hoffmann, C., Stiller, C.: Continuous stereo self-calibration by camera parameter tracking. IEEE Transactions on Image Processing 18(7), 1536–1550 (2009)
8. Schreiber, W., Notni, G.: Theory and arrangements of self-calibrating whole-body three-dimensional measurement systems using fringe projection technique. Opt. Eng. 39, 159–169 (2000)
9. Reich, C., Ritter, R., Thesing, J.: 3-D shape measurement of complex objects by combining photogrammetry and fringe projection. Opt. Eng. 39, 224–231 (2000)
10. Chen, F., Brown, G.M.: Overview of three-dimensional shape measurement using optical methods. Opt. Eng. 39, 10–22 (2000)
11. Sansoni, G., Carocci, M., Rodella, R.: Three-dimensional vision based on a combination of Gray-code and phase-shift light projection: Analysis and compensation of the systematic errors. Applied Optics 38(31), 6565–6573 (1999)
12. Thesing, J.: New approaches for phase determination. In: Proc. SPIE, vol. 3478, pp. 133–141 (1998)
13. Brown, D.C.: Close-range camera calibration. Photogram. Eng. 37(8), 855–866 (1971)
14. Bräuer-Burchardt, C.: A simple new method for precise lens distortion correction of low cost camera systems. In: Rasmussen, C.E., Bülthoff, H.H., Schölkopf, B., Giese, M.A. (eds.) DAGM 2004. LNCS, vol. 3175, pp. 570–577. Springer, Heidelberg (2004)
15. Kühmstedt, P., Bräuer-Burchardt, C., Munkelt, C., Heinze, M., Palme, M., Schmidt, I., Hintersehr, J., Notni, G.: Intraoral 3D scanner. In: Proc. SPIE, vol. 6762, 67620E (2007)